Hydrothermal Synthesis and Crystal Growth Studies of BaTiO 3 Using Ti Nanotube Precursors

ARTICLE *in* CRYSTAL GROWTH & DESIGN · SEPTEMBER 2008

Impact Factor: 4.89 · DOI: 10.1021/cg800215r

CRYSTAL GROWTH & DESIGN
2008
VOL. 8, NO. 9
3309–3315

Hydrothermal Synthesis and Crystal Growth Studies of $BaTiO_3$ Using Ti Nanotube Precursors

Florentina Maxim,[†] Paula Ferreira,[†] Paula M. Vilarinho,*[,†] and Ian Reaney[‡]

Department of Ceramics and Glass Engineering, CICECO, University of Aveiro, 3810-193 Aveiro, Portugal, and Department of Engineering Materials, University of Sheffield, Sheffield S1 3JD, United Kingdom

Received February 26, 2008; Revised Manuscript Received May 3, 2008

ABSTRACT: The hydrothermal synthesis of barium titanate particles by reaction of titanate layered nanotubes and barium hydroxide in aqueous solution at 90, 110, and 200 °C from 1 to 24 h has been studied. Anisotropic growth of barium titanate particles was observed when the synthesis temperature was 90 °C resulting in the formation of pseudo-cubic $BaTiO_3$ single-crystal particles with a "wild"-type dendritic shape. Synthesis at 110 °C led to the formation of round-shaped, pseudo-cubic, and tetragonal $BaTiO_3$ particles. At 200 °C, single-crystal barium titanate "seaweed"-type dendritic particles with predominantly tetragonal structure were obtained. This study demonstrates that the anisotropic growth of barium titanate crystals can be controlled by manipulating the temperature and time of reaction and highlights the influence of the synthesis parameters on the anisotropic growth of $BaTiO_3$ crystals under hydrothermal conditions when using layered titanates with nanotube morphology as Ti precursor.

Introduction

Above ~130 °C, $BaTiO_3$ exhibits a cubic paraelectric (PE) structure but on cooling below this temperature it distorts along the [001] direction to a ferroelectric (FE) tetragonal phase with a *c*/*a* ratio of ~1.01. $BaTiO_3$ subsequently undergoes two further FE- FE phase transitions on cooling at 0 °C and −90 °C to orthorhombic and rhombohedral structures, in which the polarization vectors lie along the [110] and [111] directions, respectively.

The conventional method of fabrication of $BaTiO_3$ is by the reaction of carbonate and oxide raw materials, $BaCO_3$ and TiO_2 at high temperature, typically around 1100 °C, which after milling gives rise to particles around 1−2 μm diameter. However, the drive to ever increasing volumetric efficiency has led to dielectric layer thicknesses in multilayer ceramic capacitors of <1 μm and a need for $BaTiO_3$ with <300 nm powder diameter. [1] More recently and motivated by the industrial need of size reduction of microelectronics devices, one-dimensional (1D) ferroelectric nanostructures (nanorods, nanotubes, nanowires) that might exhibit drastically different properties from those of the bulk counterpart are being considered.[2] However, there are few studies analyzing the influence of the shape on the ferroelectric properties.[3–5] Recently, Morozovska et al.[6] predicted the enhancement of the ferroelectric properties in one-dimensional (1D) nanorods and nanowires. Nanowires of barium titanate with ca. 1.2 nm of radius possess the minimal critical volume that allows the ferroelectricity to be conserved above room temperature ($T_C \approx 400$ K). On the other end, it is well-known that the shape and size of particles are highly dependent on the preparation method and controlled by the synthesis parameters. From this point of view, there is a strong need to develop synthetic methods to produce ferroelectric 1D nanostructures to achieve a major breakthrough in understanding the effect of scaling and dimensionality on electric properties and eventually in transferring this knowledge to practical applications.

Consequently, much recent research has centered on chemical routes for the preparation of $BaTiO_3$ powder. Several such routes have been reported in the literature and reviewed by Hennings.[7] Among these methodologies, the hydrothermal procedure has been referred to as a versatile, low cost and environmentally friendly method for the preparation of barium titanate nanoparticles with different sizes and morphologies. The hydrothermal formation of $BaTiO_3$ requires high pH (>12), because at low pH the solubility of barium titanate increases. The reaction can be carried out at lower pH but only at elevated temperature.[8] Two concurrent nucleation and growth mechanisms were proposed for the hydrothermal crystallization of barium titanate.[9–11] Hertl[10] suggested an in situ transformation model, which assumes that the dissolved Ba^{2+} and $Ba(OH)^+$ ions react topochemically with the titanium precursor and the $BaTiO_3$ is formed by heterogeneous nucleation on its surface.[10,12] The second mechanism, the dissolution−precipitation mechanism,[9,11] assumes that barium and titanium sources are rapidly dissolved and homogeneous nucleation of barium titanate takes place. The thermodynamic and kinetics of $BaTiO_3$ hydrothermal formation is principally dictated by the properties of the titanium precursor,[8–11,13–16] as most of the barium sources are readily soluble in aqueous media. Recently, layered titanates were found to act as highly reactive titanium precursors suitable for the preparation of $BaTiO_3$ particles due to their enhanced ion-exchange capacity.[12] Moreover, it has been proposed that the morphology of the layered structured titanium precursor might be maintained if the topotactic reaction mechanism is favored and enhanced.[12]

The main drawback of the application of the hydrothermal method to the synthesis of barium titanate is the difficulty of obtaining defect free crystals. The dehydration/condensation and precipitation of $BaTiO_3$ at low and moderate temperatures in the presence of water leads to partial retention of hydroxyl ions in the crystal structure. The aliovalent OH^- replacing the O^{2-} ions on the oxygen sublattice have to be compensated by an equivalent number of cation vacancies. It was suggested that the presence of these lattice defects and the accompanying microstrains are responsible for the retention of metastable cubic phase at room temperature.[13] In addition, it was demonstrated that by limiting the growth in the ⟨111⟩ direction, barium titanate particles with low defect concentration and plate like morphology (100:1 aspect ratio) could be synthesized.[17]

* Corresponding author. E-mail: paula.vilarinho@ua.pt. Tel: 351 234 370354/259. Fax: 351 234 370204.
[†] University of Aveiro.
[‡] University of Sheffield.

10.1021/cg800215r CCC: $40.75
Published on Web 07/25/2008

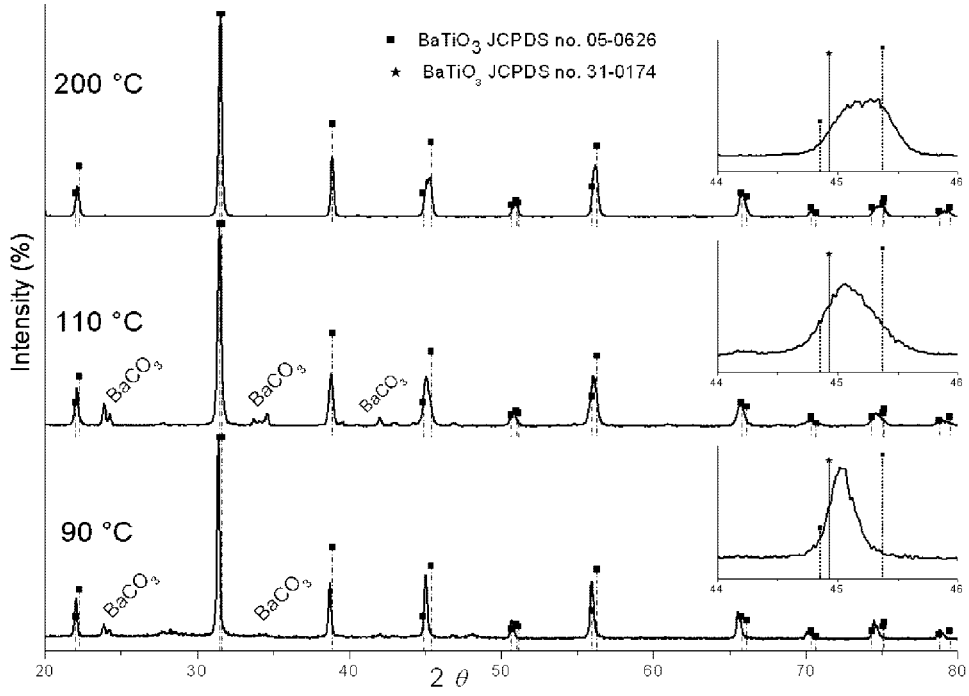

Figure 1. X-ray diffraction patterns of samples prepared at 90, 110, and 200 °C for 24 h. The insets show the reflections around 2θ of 45° [(200) and (002)].

Despite the large number of studies of hydrothermal synthesis of complex oxides, only Mao et al.[18] and Joshi et al.[19] have reported the preparation of 1D barium titanate with high aspect ratio in aqueous media. Starting with anatase nanotubes, Mao et al. detailed the preparation of cubic $BaTiO_3$ nanotubes.[18] However, the chemical nature of the nanotubes was not clearly identified and the obtained powders contained amorphous phases, unreacted titania nanotubes and carbonate impurities.[18,20] Joshi et al. obtained $BaTiO_3$ nanowires (50−200 nm) by the hydrothermal method starting from commercial TiO_2 and $Ba(OH)_2$ in the presence of ammonia.[19]

To the best knowledge of the authors, the anisotropic crystal growth of $BaTiO_3$ has not been thoroughly studied. The reasons for the lack of such studies might be related to the absence of predictive models regarding the anisotropic $BaTiO_3$ crystal growth under hydrothermal conditions. Therefore, it is necessary to define empirically the fundamental role of the synthesis parameters (temperature, pressure, precursor, time) on the crystallization thermodynamics and kinetics of anisotropic growth of barium titanate.

As $BaTiO_3$ hydrothermal formation is essentially dictated by the properties of the titanium precursor, the main objective of this work is to evaluate the influence of synthesis temperature and time on the crystallographic phase and on the anisotropic growth of barium titanate crystals under hydrothermal conditions when using layered titanates with nanotubular morphology as the titanium precursor. The structural evolution of the obtained $BaTiO_3$ powders was followed by X-ray diffraction and Raman spectroscopy and morphological characterization was performed using SEM and TEM/HRTEM.

Experimental Section

All the syntheses were performed in Teflon lined autoclaves. A layered titanate precursor with the general formula $Na_{2-x}H_xTi_2O_5 \cdot 1.8H_2O$ and $Ba(OH)_2 \cdot 8H_2O$ (Merck, 98% purity) were used as titanium and barium source, respectively. The Ti precursor was made by mixing 2 g of anatase (Merck, 99%) with 40 mL of 10 M NaOH (Fluka, 97%) solution. After stirring, the mixture was autoclaved for 48 h at 150 °C. The product was filtered, washed with distilled water until pH 7 and dried at 60 °C. The detailed preparation of the titanium precursor is reported elsewhere.[21]

The barium titanate preparation was initiated by mixing barium and titanium precursors in a 1.01 Ba/Ti molar ratio with the necessary quantity of deionized distilled water in order to prepare a 0.1 M solution of $Ba(OH)_2$. In this way, the pH of the starting mixture was above 13. These experimental conditions were chosen based on the thermodynamic studies of Lencka et al.[8] After stirring for 30 min, the mixtures were transferred into Teflon-lined autoclaves and the hydrothermal syntheses were performed at 90, 110 and 200 °C for several periods of time. Following the synthesis the products were washed with distilled water for various times and dried overnight at 50 °C. For simplification the samples are identified with BT and two numbers indicating the temperature and time of synthesis. For example, the sample prepared at 90 °C for 24 h was indexed as BT9024.

The phase identification of the obtained samples was conducted with powder X-ray diffraction (XRD) on a Rigaku diffractometer using Cu Kα radiation filtered by Ni. The diffraction patterns were acquired from 15 ° to 130 ° (2θ) with a step length of 0.02 and a fixed counting time of 7 s. The X-ray patterns where characterized afterward using *Jade* software.[22] As a supplementary method for the phase identification Raman spectroscopy was utilized. Raman spectra were recorded on a Bruker RFS 100/S FT Raman spectrometer using a 1064 nm excitation of the Nd/YAG laser.

The microstructures were analyzed by scanning electron microscopy (SEM), with a Hitachi SU-70 (S-4100) microscope, and by transmission electron microscopy (HRTEM) with a 300 eV Hitachi H9000-NA instrument.

Results

Influence of Temperature. Figure 1 presents the X-ray diffraction patterns of the samples prepared at 90, 110 and 200 °C for 24 h. All the samples can be indexed with both tetragonal (JCPDF 05−0626) and cubic (JCPDF no. 31−0174) $BaTiO_3$ structures. The X-ray pattern of the sample obtained at 90 °C indicate that barium titanate is predominantly cubic (c/a = 1.0005). An increase in the tetragonality is noted when the synthesis temperature increased to 110 and 200 °C (c/a =

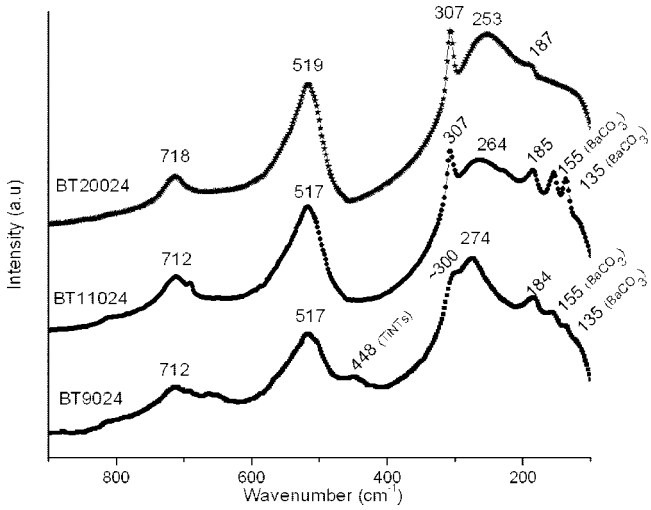

Figure 2. Raman spectra of samples prepared at 90, 110, and 200 °C for 24 h.

1.006). The insets in Figure 1 show the reflections around 2θ of 45° [(200) and (002)] denoting the splitting of the peaks in this region as a result of the distortion of the unit cell, characteristic of the tetragonal structure. As a comparison the (200) reflection of cubic $BaTiO_3$ (JCPDF 31−0174) is also presented. In addition, it can be observed (Figure 1) that the samples prepared at 90 and 110 °C for 24 h contain residual $BaCO_3$. No $BaCO_3$ was obtained after 24 h of reaction at 200 °C.

Figure 2 shows the Raman spectra of the samples prepared at 90, 110 and 200 °C for 24 h. Eight Raman active modes are expected for tetragonal $BaTiO_3$ with a space group *P*4*mm*, $3A_{1\,g} + B_{1\,g} + 4E_g$.[23] The peaks at around 517, 253, and 185 cm^{-1} are assigned to the fundamental TO modes (transverse component of the optical mode) of A1 symmetry and the peak at 307 cm^{-1} is assigned to the B1 mode, indicating an asymmetry within the TiO_6 octahedra of $BaTiO_3$ on a local scale. The broadband at around 715 cm^{-1} is related to the highest frequency longitudinal optical mode (LO) of A1 symmetry. If the sharpness of the peak at 307 cm^{-1} is reduced and it becomes indistinct then the tetragonal phase is not dominant.[24] The sample synthesized at 90 °C presents bands at around 184, 274 (a small shoulder at ∼ 300), 448, 517, 663, and 712 cm^{-1}. Increasing the synthesis temperature to 110 °C sharp bands at 136, 154, 185, 307, and 517 cm^{-1} appeared. Two broad peaks at 264 and 712 cm^{-1} were also present. The sample obtained at 200 °C contained peaks of predominantly tetragonal barium titanate identified by the bands around 184 (shoulder), 253 (broad), and the three sharp peaks at 307, 519, and 718 cm^{-1}.[25] The main difference between the Raman spectra of these samples consists in a band shift from 274 cm^{-1} for the sample prepared at 90 °C to lower frequencies, to 264 cm^{-1} for the sample prepared at 110 °C, and to 253 cm^{-1} for the sample prepared at 200 °C.

Figure 3 shows SEM images of (a) titanium precursor (Ti-A) and the barium titanate samples obtained after 24 h at (b) 90 °C (BT9024), (c) 110 °C (BT11024), and (d) 200 °C (BT20024). It can be readily noticed the modification of the titanium precursor initial morphology during its hydrothermal treatment. When the synthesis temperature is 90 and 200 °C, dendritic morphologies are observed. Partially disordered dendrites with mostly planar structure are detected for the samples prepared at 90 °C. The average dendron size is ∼2.5 μm in length and ∼200 nm in diameter with a rough surface. Unreacted precursor can be also noticed. In the case of the samples prepared at 200 °C, the frequency of dendritic branching increased resulting in three-dimensional aggregates of disordered dendrites. The surfaces of the dendrons are smooth and the average dendron length is ∼1 μm and the diameter is ∼150 nm. The situation is completely different when the synthesis is performed at 110 °C. A general low-magnification view reveals round-shaped particles with small sizes (∼ 80 nm), but the inset of Figure 3c shows regions of inhomogeneous growth with the nucleation of branching structures.

The TEM images of the sample prepared at 90 °C are presented in Figure 4. The dark field TEM image (Figure 4a) suggests, as anticipated, that each dendrite is a single crystal. EDS reveals that the particles are composed of Ba, Ti and O (see Figure 4a, down inset). A faceted growth of the dendrons is evidenced in the bright field TEM image of the same sample (Figure 4b). It is also indicated that the angle between the "mother" dendron and the "daughter" dendron[26] is 90°. This result is corroborated by the selected area electron diffraction (SAED) pattern (see inset in Figure 4b) that demonstrates that the crystal growth directions are along the ⟨001⟩ direction of the cubic lattice. This is typical for growth perovskite crystals where the A and B cations have 2^+ and 4^+ valence states, respectively, because the {001} facets are neutral and have the lowest interfacial energy with the surrounding media.

The morphology of the particles prepared at 200 °C for 24 h was also analyzed by TEM and is shown in Figure 5. Differences in contrast along the seaweed dendron can be detected, but SAED patterns taken from multiple locations of the dendrons (see inset of Figure 5a) indicate only slight changes in orientation on the order of 1−2 degrees. It is concluded therefore that they are essentially single crystals. In addition, "daughter" dendrons once again grow perpendicular to the "mother", suggesting a crystal axis orientation growth along the ⟨001⟩ directions, Figure 5b.

Influence of Time. At 90 °C hydrothermal treatment, X-ray diffraction revealed $BaTiO_3$ was absent until 24 h of reaction time. This is in contrast with hydrothermal treatment at 200 °C, at which temperature the $BaTiO_3$ phase is formed after 1 h. However, a substantial quantity of $BaCO_3$ is residual, which decreases monotonously until only $BaTiO_3$ is present by XRD after 24 h.

Figure 6 presents the Raman spectra of the samples prepared at 90 °C for 1 h (BT901), 12 h (BT9012), and 24 h (BT9024). The spectra of titanium precursor (denominated as Ti-A) is also shown for comparison. The Raman spectra of samples collected after 1 and 12 h show the characteristic bands of the titanium precursor at around 166, 191, 276, 450, 663 cm^{-1}, and a broad peak at ∼910 cm^{-1}.[27] When comparing the Raman spectra of titanium precursor with the one of BT901 sample, we can notice the appearance of two new bands at around 135 and 155 cm^{-1}, which according to Shiratori et al.[28] can be assigned to orthorhombic $BaCO_3$. The spectra of samples collected after 24 h of reaction show the characteristic bands of barium titanate (185, shoulder at ∼300, 516, 715 cm^{-1}). It is worth noting here that the characteristic band at 276 cm^{-1} of titanium precursor does not change during the reaction for all the samples prepared at 90 °C suggesting a slow conversion to $BaTiO_3$.

Figure 7 presents the Raman spectra of the equivalent samples prepared at 200 °C. The spectra of samples obtained after 6 and 24 h are similar with characteristic bands of tetragonal

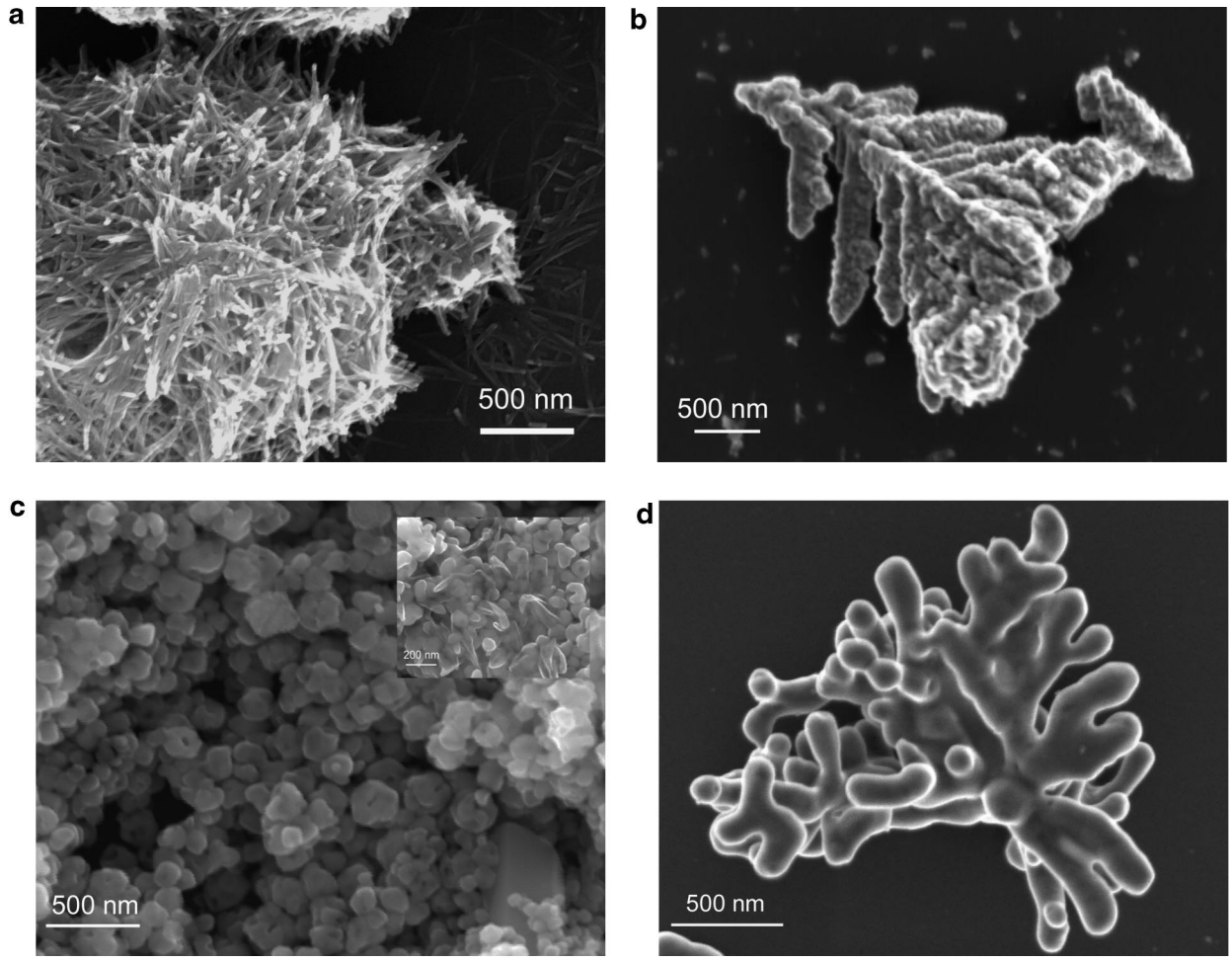

Figure 3. SEM images of (a) titanium precursor (Ti-A) and the barium titanate samples obtained after 24 h at (b) 90 °C (BT9024), (c) 110 °C (BT11024), and (d) 200 °C (BT20024). The inset in Figure 3c shows a close view of sample BT11024.

barium titanate at around 184 (shoulder), 253 (broad) and three sharp peaks at 307, 516, and 715 cm^{-1}. Besides these bands, the BT2001 sample also has the characteristic bands associated with anatase,[29] specifically the sharp band at 144 cm^{-1} and the two broad bands at around 400 and 640 cm^{-1}. Because of the presence of barium carbonate, the formed anatase is not clearly detected by XRD.

No morphological differences were apparent for the samples prepared at 90 °C when examined by SEM and TEM. However, obvious differences were observed for the samples prepared at 110 °C for different synthesis times. Figure 8 depicts the SEM images of samples prepared at 110 °C for 144 h (BT110144). After 24 h, mostly round-shaped particles were obtained, as shown in Figure 3c), in which an incipient dendritic growth is suggested. The dendritic growth becomes obvious after 144 h at this temperature. Figure 9 presents the SEM images of samples prepared at 200 °C for 1 and 6 h respectively. The sample obtained after 1 h (Figure 9a) shows two morphologies: small particles with round shape and big plate like particles. A better view obtained by TEM of the round-shaped particles with ~110 nm in size is presented in the inset of Figure 9a. The chemical composition determined by EDS (not shown) indicates that the small particles are $BaTiO_3$ and the big particles are $BaCO_3$. After 6 h of reaction (Figure 9b) the big particles remain present in the sample, the small particles are not observed anymore but seaweed[26] dendritic particles with a dendron diameter of ~175 nm appeared.

Discussion

The results presented above show that crystalline $BaTiO_3$ can be prepared at temperatures ranging from 90 to 200 °C by hydrothermal treatment using layered nanotubes and $Ba(OH)_2$ as Ti and Ba sources, respectively. However, there is a marked difference in morphology of the particles depending on the temperature and reaction time. Low temperatures (90 °C) favor rough dendrites, whereas at 110 and 200 °C, either round-shaped particles or dendrites are observed. There is no resemblance with the microstructures reported by Mao's group.[18]

Hertl,[10] in part, explained some of the observed differences by considering that the solubility of the Ti precursor increases with increasing temperature. He postulated that at some critical temperature (>90 °C in this study), the Ti precursor dissolves prior to reaction with $Ba(OH)_2$. Below this value the mechanism is topochemical and $BaTiO_3$ effectively grows on the surface of the Ti precursor. In the first hours of topochemical synthesis, Ba^{2+} ions partially exchange with Na^+ and proton ions existent between the nanotube layers are also adsorbed at the surface of the titanate nanotubes. The formation of $BaTiO_3$ occurs simultaneously with dehydration, which is a slow process in superheated fluids.[13] Residual hydroxyl ions are retained in the oxygen sublattice and are compensated by cation vacancies.

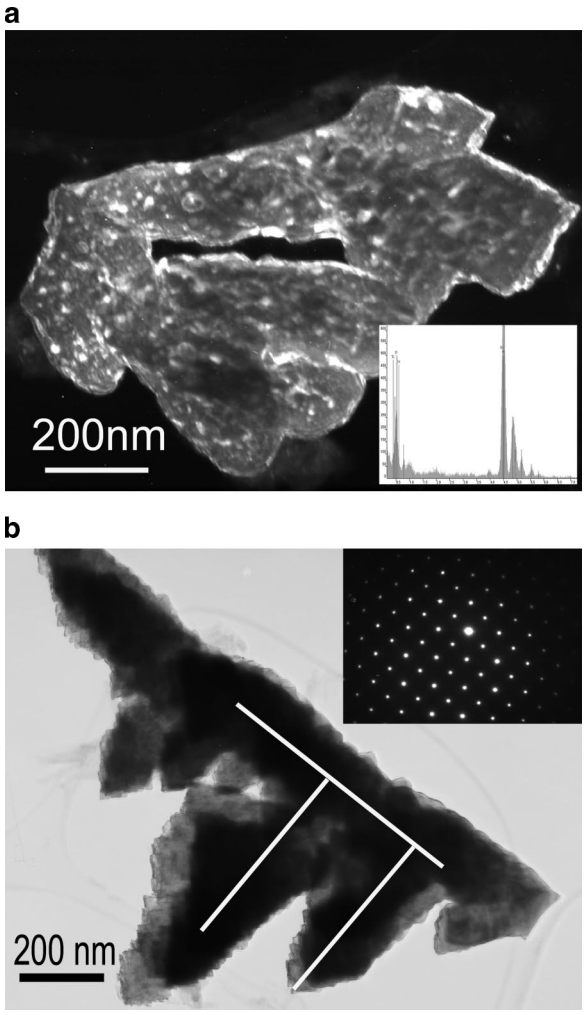

Figure 4. TEM images of samples prepared at 90 °C (BT9024): (a) dark field; the down inset shows the EDS pattern; (b) bright filed; the inset displays the selected area electron diffraction.

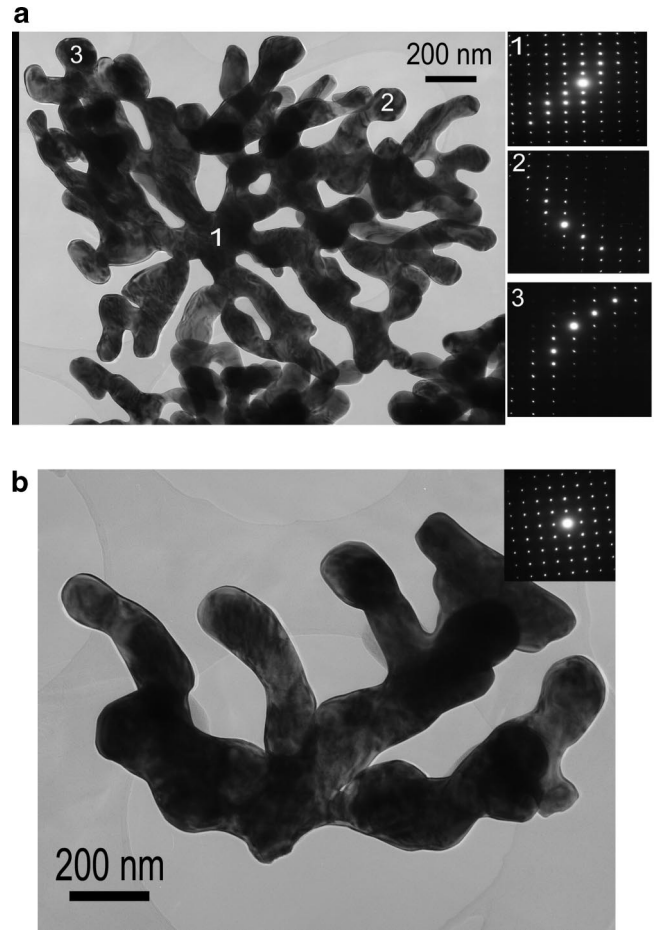

Figure 5. TEM images (a) and (b) of samples prepared at 200 °C (BT20024). The insets displays the selected area electron diffraction in the indicated points.

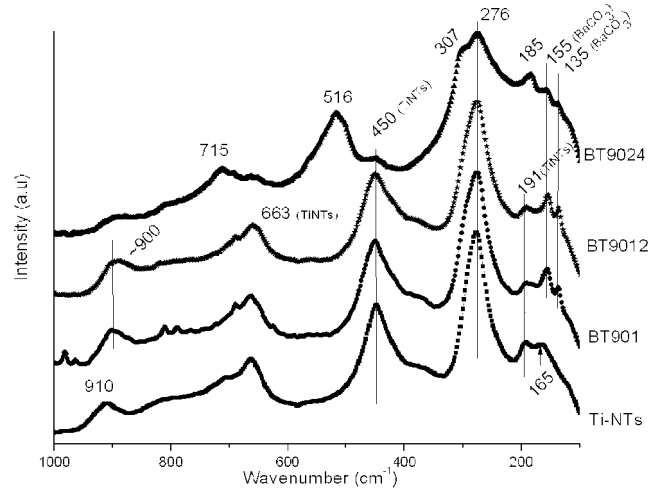

Figure 6. Raman spectra of samples prepared at 90 °C for 1 (BT901), 12 (BT9012), and 24 h (BT9024). The Raman spectra of the titanium precursor (Ti-A) is presented for comparison reasons.

These lattice defects lead to the presence of a metastable $BaTiO_3$ pseudo-cubic phase at room temperature, as stated by Vivekanandan et al.[13] The presence of defects on the crystal lattice can be supported by the single diffraction peak at 45° 2θ (Figure 1) and by the absence of a clear band at 307 cm^{-1} (characteristic of tetragonal $BaTiO_3$) in the Raman spectrum (Figure 2).

For reactions at >90 °C, the Ti precursors dissolve creating Ti rich regions in the aqueous medium which acts as a nucleation site for $BaTiO_3$.[9] The mechanism of dissolution appears to occur via an intermediate anatase phase formed by the dehydration of the nanotubes after 1 h thermal treatment at 200 °C (Figure 7). Subsequently, the Ti−O bonds of the anatase are broken by hydrolytic reaction to form a $[Ti(OH)_x^{4-x}]$ soluble species that reacts with the Ba^{2+} and $BaOH^+$ ions in solution to precipitate $BaTiO_3$. The high solubility of the Ti precursor may be attributed to the layered structure of the titanate nanotubes which originates from a zigzag chainlike structure of the basic structural TiO_6 octahedral units.[30] Within the layers, Na^+ or H^+ ions exist to balance the electric charge leaving the nanotubes vulnerable to a particularly high ion-exchange capacity and degree of hydration in aqueous media at low temperature.[31] Similar levels of solubility where achieved by Clark et al.[32] who utilized an amorphous Ti precursor (H_2TiO_3), commercially referred to as titanic acid.

At 110 °C, round-shaped particles (80 nm) are generally observed after 24 h (Figure 3c) (although some preliminary branching is evident (see inset of Figure 3c) whereas at 200 °C large single-crystal dendrites (1 μm) with rounded arms are present (Figure 3d). From a simplistic perspective, these two conditions (110 and 200 °C) appear to correspond to two

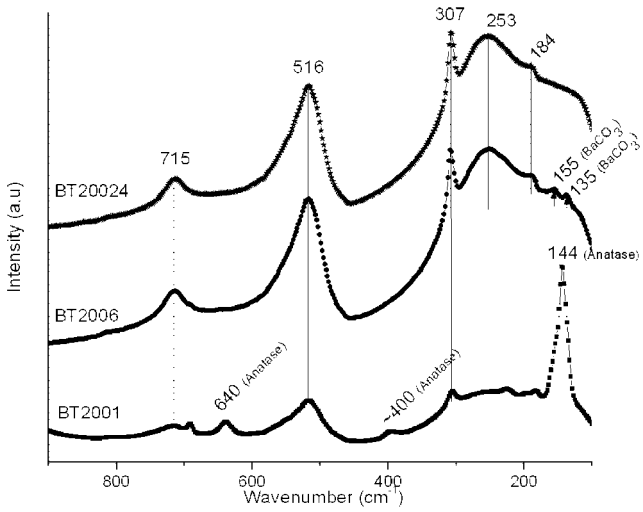

Figure 7. Raman spectra of samples prepared at 200 °C for 1 (BT2001), 6 (BT2006), and 24 h (BT20024).

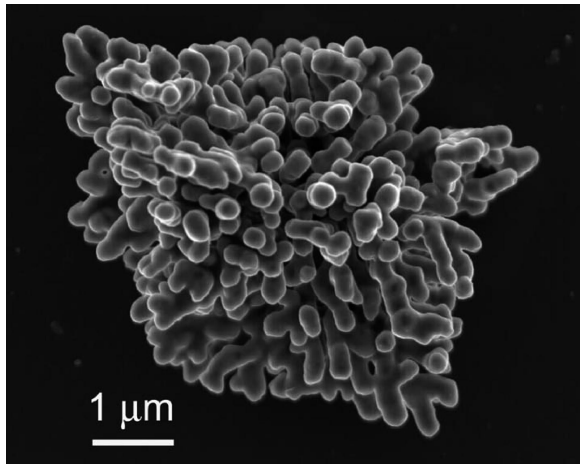

Figure 8. SEM image of the sample prepared at 100 °C for 144 h (BT110144).

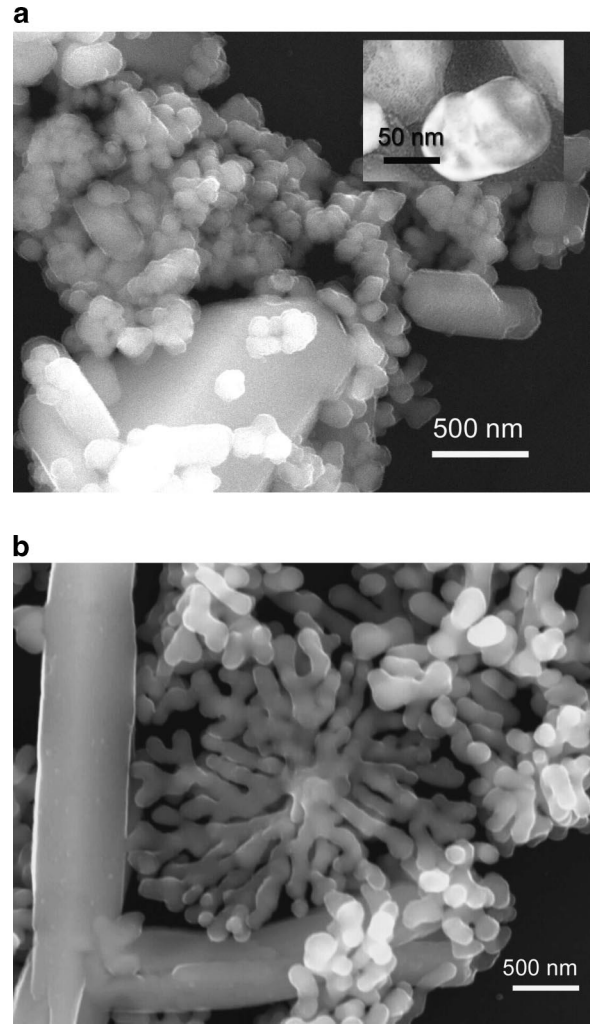

Figure 9. SEM images of sample prepared at 200 °C for (a) 1 (BT2001) and (b) 6 h (BT2006).

different regimes for the precipitation of $BaTiO_3$. At 110 °C, the crystals are formed in a temperature regime where nucleation dominates within the aqueous medium and growth of the $BaTiO_3$ particles is restricted. Conversely, at 200 °C, growth dominates and upon formation of a stable nucleus a large dendritic crystal rapidly forms. The presence of round-shaped particles after 2 h at 200 °C confirms this hypothesis; the reaction to form $BaTiO_3$ is incomplete and only nuclei that will ultimately grow to form the dendrites are present.

The large number of defects present at the $BaTiO_3$ nucleus creates a high surface energy and a strong anisotropic curvature of the surface, giving rise to high surface tension anisotropy of the solid−liquid interface. Together with a diffusion-limited aggregation phenomena, surface tension anisotropy is the driving force for the observed dendritic growth. In this work, two types of dendrites are observed: (i) the wild-type dendritic growth as in the particles prepared at 90 °C (Figures 3b and 4) and (ii) the seaweed-type dendritic growth obtained for particles synthesized at 200 °C (Figures 3d and 5).

At 90 °C, the $BaTiO_3$ nuclei, obtained mainly by the topochemical reaction mechanism on the nanotube surface, possess a high concentration of lattice defects. Molecular motion is limited and dendritic growth is consequently controlled by the high surface energy. Consequently, a rough surface with faceted growth (wild type dendritic growth) is observed (Figures 3b and 4). At 200 °C, a combination of relatively fast molecular motion and the occurrence of a dissolution −precipitation mechanism, results in fewer surface defects and a lower surface energy. The growth of "daughter" dendrons is favored and the sharp tips of the dendrons are eliminated. Under such conditions, seaweed-type dendritic particles with smooth surfaces are formed (Figures 3d and 5).

The round-shaped particles obtained at 110 °C after 24 h (Figure 3c) are similar to the ones observed for samples prepared at 200 °C after 1 h (Figure 9a). It is believed, therefore, that they represent the early stages of the dissolution−precipitation reaction in which the round-shaped particles are effectively nuclei for subsequent dendritic growth. Similar, but less extreme conditions for growth occur at 110 °C (Figure 3c) as opposed to 200 °C and therefore after prolonged thermal treatment at 110 °C (Figure 8) some evidence of burgeoning dendrites are observed that appear to possess seaweed type branches (Figure 3c).

Conclusions

Anisotropic $BaTiO_3$ nanoparticles were successfully prepared by hydrothermal synthesis in the temperature range from 90 to 200 °C starting from layered titanate nanotubes of general

formula $Na_{2-x}H_xTi_2O_5 \cdot 1.8H_2O$. The mechanism of barium titanate crystallization depends on the temperature of synthesis and reflects the properties of the titanium precursor. Pseudocubic single-crystalline $BaTiO_3$ particles form at 90 °C, as a result of an in situ topotactic reaction. Above 90 °C, dissolution of the nanotubes ensues and the $BaTiO_3$ forms via precipitation. At 110 °C, the formation of $BaTiO_3$ is dominated by nucleation with limited growth hence small round-shaped precipitates are generally observed. At 200 °C, however, growth is rapid once $BaTiO_3$ has nucleated and a dendritic morphology ensues.

These results strongly question the use of layered titanate NTs as templates to promote the formation of barium titanate perovskite NTs. The topochemical reaction to form $BaTiO_3$ at 90 °C is most likely to retain the NT morphology but no evidence of its retention was observed in this study. Moreover, above 90 °C, dissolution of layered titanate NTs occurs followed by precipitation of $BaTiO_3$; a mechanism that nullifies any potential template effect.

Acknowledgment. The authors acknowledge FCT, FEDER, and European Network of Excellence FAME, under Contract FP6-500159-1. F.M. is thankful to FCT for the fellowship SFRH/BD/23375/2005.

References

(1) Pithan, C.; Hennings, D.; Waser, R. *Int. J. Appl. Ceram. Technol.* **2005**, *2*, 1–14.
(2) Xia, Y.; Yang, P.; Sun, Y.; Wu, Y.; Mayers, B.; Gates, B.; Yin, Y.; Kim, F.; Yan, H. *Adv. Mater.* **2003**, *15*, 353–389.
(3) Spanier, J. E.; Kolpak, A. M.; Urban, J. J.; Grinberg, I.; Ouyang, L.; Yun, W. S.; Rappe, A. M.; Park, H. *Nano Lett.* **2006**, *6*, 735–739.
(4) Urban, J. J.; Yun, W. S. G. Q. P. H. *J. Am. Chem. Soc.* **2002**, *124*, 1186–1187.
(5) Urban, J. J.; Spanier, J. E.; Ouyang, L. Y. W. S.; Park, H. *Adv. Mater.* **2003**, *15*, 423–426.
(6) Morozovska, A. N.; Eliseev, E. A.; Glinchuk, M. D. *Physica B* **2007**, *387*, 358–366.
(7) Hennings, D. *Br. Ceram. Proc.* **1989**, *41*, 1–10.
(8) Lencka, M. M.; Riman, R. E. *Chem. Mater.* **1993**, *5*, 61–70.
(9) Eckert, J. O., Jr.; Hung-Houston, C. C.; Gersten, B. L.; Lencka, M. M.; Riman, R. E. *J. Am. Ceram. Soc.* **1996**, *79*, 2929–2939.
(10) Hertl, W. *J. Am. Ceram. Soc.* **1988**, *71*, 879–883.
(11) Testino, A.; Buscaglia, V.; Buscaglia, M. T.; Viviani, M.; Nanni, P. *Chem. Mater.* **2005**, *17*, 5346–5356.
(12) Feng, Q.; Hirasawa, M.; Yanagisawa, K. *Chem. Mater.* **2001**, *13*, 290–296.
(13) Vivekanandan, R.; Kutty, T. R. N. *Powder Technol.* **1989**, *57*, 181–192.
(14) Hennings, D.; Rosenstein, G.; Schreinemacher, H. *J. Eur. Ceram. Soc.* **1991**, *8*, 107–115.
(15) Moon, J.; Kerchner, J. A.; Krarup, H.; Adair, J. H. *J. Mater. Res.* **1999**, *14*, 425–435.
(16) Viviani, M.; Buscaglia, M. T.; Testino, A.; Buscaglia, V.; Bowen, P.; Nanni, P. *J. Eur. Ceram. Soc.* **2003**, *23*, 1383–1390.
(17) Yosenick, T. J.; Miller, D. V.; Kumar, R.; Nelson, J. A.; Randall, C. A.; Adair, J. H. *J. Mater. Res.* **2005**, *20*, 837–843.
(18) Mao, Y.; Banerjee, S.; Wong, S. S. *Chem. Commun.* **2003**, *408*, 409.
(19) Joshi, U. A.; Lee, J. S. *Small* **2005**, *1*, 1172–1176.
(20) Mao, Y.; Park, T.-J.; Zhang, F.; Zhou, H.; Wong, S. S. *Small* **2007**, *3*, 1122–1139.
(21) Maxim, F.; Ferreira, P.; Vilarinho, P. M. submitted.
(22) *JADE*, version 5.0; Materials Data Inc.: Livermore, CA, 2004.
(23) Asiaie, R.; Zhu, W.; Akbar, S. A.; Dutta, P. K. *Chem. Mater.* **1996**, *8*, 226–234.
(24) Joshi, U. A.; Yoon, S.; Balk, S.; Lee, J. S. *J. Phys. Chem. B* **2006**, *110*, 12249–12256.
(25) Begg, B. D.; Finnie, K. S.; Vance, E. R. *J. Am. Ceram. Soc.* **1996**, *79*, 2666–2672.
(26) Karma, A. Lectures on Dendritic Growth. In *Branching in Nature*; Fleury, V., Gouyet, J. F., Leonetti,M., Eds.; Springer-Verlag: Weinheim, Germany, 2001; pp 365−401.
(27) Kasuga, T.; Hiramatsu, M.; Hoson, A.; Sekino, T.; Niihara, K. *Adv. Mater.* **1999**, *11*, 1307–1311.
(28) Shiratori, Y.; Pithan, C.; Dornseiffer, J.; Waser, R. *J. Raman Spectrosc.* **2007**, *38*, 1288–1299.
(29) Qian, L.; Du, Z.-L.; Yang, S.-I.; Jin, Z. *J. Mol. Struct.* **2005**, *749*, 103–107.
(30) Tsai, C.-C.; Teng, H. *Chem. Mater.* **2006**, *18*, 367–373.
(31) Sasaki, T.; Watanabe, M. *J. Am. Chem. Soc.* **1998**, *120*, 4682–4689.
(32) Clark, I. J.; Takeuchi, T.; Ohtori, N.; Sinclair, D. C. *J. Mater. Chem.* **1999**, *9*, 83–91.

CG800215R